Mon. Not. R. Astron. Soc. **298,** 378–386 (1998)

Angular correlations between LBQS and APM: weak lensing by the large-scale structure

Liliya L. R. Williams[1⋆] and Mike Irwin[2⋆]
[1]*Institute of Astronomy, Madingley Road, Cambridge CB3 0HA*
[2]*Royal Greenwich Observatory, Madingley Road, Cambridge CB3 0EZ*

Accpeted 1998 March 6. Received 1998 March 5; in original form 1997 December 3

ABSTRACT

We detect a positive angular correlation between bright, high-redshift QSOs and foreground galaxies. The QSOs are taken from the optically selected LBQS Catalogue, while the galaxies are from the APM Survey. The correlation amplitude is about a few per cent on angular scales of over a degree. It is a function of QSO redshift and apparent magnitude, in a way expected from weak lensing, and inconsistent with QSO–galaxy correlations being caused by physical associations, or uneven obscuration by Galactic dust. The correlations are ascribed to the weak lensing effect of the foreground dark matter, which is traced by the APM galaxies. The amplitude of the effect found here is compared to the analytical predictions from the literature, and to the predictions of a phenomenological model, which is based on the observed counts-in-cells distribution of APM galaxies. While the latter agree reasonably well with the analytical predictions (namely those of Dolag & Bartelmann and Sanz et al.), both underpredict the observed correlation amplitude on degree angular scales. We consider the possible ways to reconcile these observations with theory, and discuss the implications that these observations have on some aspects of extragalactic astronomy.

Key words: surveys – galaxies: general – quasars: general – gravitational lensing – large-scale structure of Universe.

1 INTRODUCTION

It is now widely recognized that the sky-projected density of high-redshift objects can be altered due to weak lensing by intervening mass distribution, on a range of angular scales (Narayan 1989; Broadhurst, Taylor & Peacock 1995). The effect arises because gravitational lensing distorts the area on the sky in the direction of the lens. Behind a lens of a positive mass density, the area is stretched out. As a result, (1) individual sources subtend a larger area on the sky and therefore look brighter due to flux conservation, but (2) their number density decreases. If the slope of magnitude number counts is steep, then the first effect wins over the second, and the net number density of background sources in a flux-limited survey is increased; if the slope is shallow, the number density is decreased. Thus the amplitude of the effect depends on the amount and clumpiness of the lensing matter, the relative redshifts of the lenses and sources, and the slope of the source number counts in the appropriate redshift range.

The effect of dilution or enhancement of the projected number density is most pronounced for sources with magnitude–number counts whose slope deviates strongly from $\alpha = \mathrm{d}\log N/\mathrm{d}m$ of 0.4. In the cases where the slope is shallower than 0.4, anticorrelations with foreground lenses have been observed or suspected: Rodrigues-Williams & Hogan (1994) suggest that the anticorrelation of faint UVX objects with clusters (Boyle, Fong & Shanks 1988) are due to weak lensing rather than dust. Broadhurst (1994) observe a deficit of faint red galaxies ($\alpha \approx 0.3$) behind the foreground cluster Abell 1689.

When the slope is steeper than 0.4, positive correlations are detected. These observations can be roughly categorized by the angular scale of correlations. On small scales, 3–30 arcsec, there are a number of observations (see Hewett, Harding & Webster 1991 and Narayan 1991 for reviews). Although direct comparison between these is difficult, because each sample has its own selection criteria and method of analysis, the correlations are thought to be reasonably well understood in terms of lensing by individual galaxy dark matter haloes.

On 1–15 arcmin scales the correlations are due to dark matter associated with galaxies, or clusters of galaxies, on Mpc scales. Such correlations with radio sources are well documented. $z > 0.5$, 1-Jy Catalogue sources have been cross-correlated with almost every available catalogue of 'low-redshift' extragalactic objects: Lick galaxies (Fugmann 1990; Bartelmann & Schneider 1993), *IRAS* galaxies and EMSS (Bartelmann & Schneider 1994), *ROSAT* All-Sky Survey (Bartelmann, Schneider & Hasinger 1994), Zwicky clusters (Seitz & Schneider 1995), APM galaxies (Benítez, N. &

⋆ E-mail: llrw@ast.cam.ac.uk (LLRW); mike@ast.cam.ac.uk (MI)

Martínez-Gonzáles 1995, 1997) and Abell clusters (Wu & Han 1995). In all instances positive correlations were found, though at varying statistical significance, from 1.5 to $\gtrsim 3\sigma$. The large amplitude of the effect remained unexplained until recently. Dolag & Bartelmann (1997) and Sanz, Martínez-Gonzáles & Benítez (1998) reproduced the correlations on $\sim$10-arcmin scales by incorporating the non-linear growth of the matter power spectrum in the Universe. Including these mass fluctuations leads to an order of magnitude increase in the QSO–galaxy correlations on Mpc scales.

On yet larger scales, 20 arcmin to 1°, there are three existing studies with homogeneous complete catalogues of objects. Rodrigues-Williams & Hogan (1994) looked at correlations between LBQS QSOs (Hewett, Foltz & Chaffee 1995) and Zwicky galaxy clusters, and found a significant signal with a subset of QSOs at $1.4 \leq z \leq 2.2$. Seitz & Schneider (1995) extended the study to 1-Jy radio sources, and a range of QSO subsamples based on redshift and apparent magnitude; sources at $z \sim 1$ were found to be associated with foreground clusters at 97.7 per cent significance level. While Rodrigues-Williams & Hogan argue that the correlations could not be the result of patchy obscuration by the Galactic dust, the study of Seitz & Schneider, who used radio selected sources, proved so beyond a doubt. The physical nature of associations can be definitely ruled out on the basis of the discrepant redshifts of QSOs and clusters, leaving weak gravitational lensing as the only plausible explanation. Ferreras, Benítez & Martínez-González (1997) detect a strong QSO–galaxy anticorrelation between faint, $z < 1.6$, optically selected QSOs in a 5.5 deg^2 region close to the North Galactic Pole. The authors attribute the effect to the selection biases associated with identifying QSOs in crowded areas.

In this paper we extend the previous work by examining the correlations between optically selected QSOs and foreground galaxies, on scales of up to 1°. In the following sections we measure the QSO–galaxy cross-correlation signal (Section 3), compare it to theoretical predictions (Section 4), and discuss a few areas of cosmology that our observations will have a considerable impact on (Sections 5 and 6).

2 DATA

The Large Bright Quasar Survey (LBQS) (Hewett et al. 1995) is the largest homogeneous catalogue of optically selected QSOs. Candidates were obtained from machine-scanned direct and objective-prism UK Schmidt Telescope plates, based on several selection criteria, including blue colour excess and presence of strong emission lines. The final list of QSOs was compiled after spectroscopic follow-up of the candidates at the Multiple Mirror and other telescopes. The LBQS contains over a 1000 QSOs between $m_B = 16$ and $\approx$18.5 in 18 fields at high Galactic latitude. The QSO redshift distribution, presented in fig. 9 of Hewett et al. (1995), is smooth and contains no gaps in the redshift range between 0.2 to 3.5. In the present work we use only the 11 equatorial LBQS fields. We do not use four fields in the direction of the Virgo cluster, because the faint galaxy counts in these fields can be severely contaminated by the Virgo galaxies. We no not use two fields in the direction of the Galactic bulge because of star contamination. We also did not use one field near the South Galactic Pole.

The APM Catalogue (Irwin, Maddox & McMahon 1994) was compiled from the scans of Schmidt plates, carried out by the Automatic Plate Measuring (APM) facility at Cambridge. This catalogue is a list of objects, detected on red and blue plates separately, and classified on the basis of their morphology as star-like, extended, noise, or blend. The galaxy data we use are only approximately magnitude-calibrated; two fields can be offset by as much as 1 mag. However, we do not attempt to correct for this, because the difference is not large for our purposes, and our analysis compensates for it.

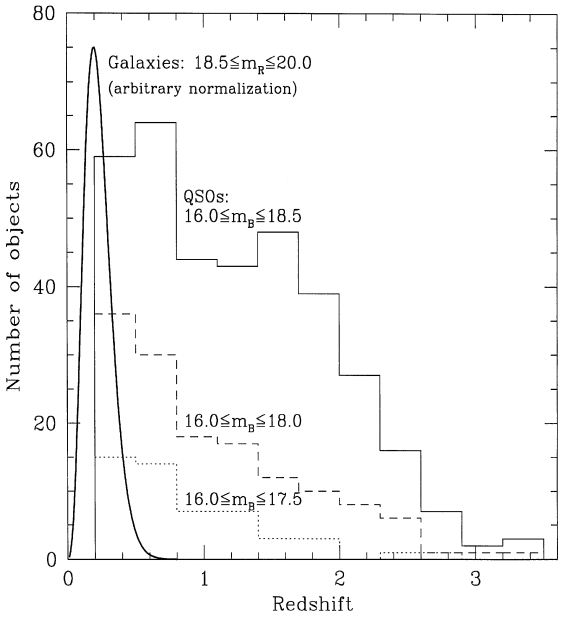

Figure 1. Redshift distribution of the objects used in the present work. The three histograms are for QSOs with $m_B \leq 17.5$, 18.0 and 18.5, all taken from 11 LBQS equatorial fields. The solid line is the estimated redshift distribution (Maddox et al. 1996) for $18.5 \leq m_R \leq 20.0$ APM galaxies (arbitrary vertical normalization).

Each Schmidt plate is $\approx$6° across, but in order to reduce vignetting problems we use only objects located within 2.°7 of the plate centre.

Fig. 1 shows the redshift distribution of LBQS QSOs and the APM galaxies. The QSOs (three histograms for $m_B \leq 17.5$, 18.0 and 18.5) are those found in 11 equatorial fields used in this work. The solid curve represents $18.5 \leq m_R \leq 20.0$ galaxies, and is based on the redshift distribution estimated by Maddox, Efstathiou & Sutherland (1996). Because the latter analysis applies to APM galaxies detected on the blue plates while we use mostly red plates, we assumed a uniform colour transformation of $B - R = 1.5$, which is the average colour of the $18.5 \leq m_R \leq 20.0$ galaxies detected on both red and blue APM plates. It is also consistent with the $B - R$ colour derived by Metcalfe et al. (1995). The peak of the galaxy redshift distribution is at $z \approx 0.2$, and virtually no galaxies lie beyond $z = 0.7$.

3 QSO–GALAXY CORRELATIONS

In this section we ask ourselves if the sky-projected distributions of the APM galaxies and background LBQS QSOs are correlated. The amplitude of the signal, if any, is expected to be small, and so it is important to take into account any possible biases that may affect the signal. In particular, Schmidt plates suffer from radial sensitivity gradients, mainly caused by vignetting, which results in radially dependent object number density. These gradients are small, and can be different for stars versus galaxies, and for faint versus bright objects. Our cross-correlation analysis, which we describe in the next section, takes these effects into account.

3.1 Method – cross-correlation estimator

The standard measure of the clustering of objects is the two-point correlation function. The commonly considered case, the autocorrelation function of galaxies, has been explored in the literature in great depth; Peebles (1980), Hewett (1982) and Hamilton (1993) have derived estimators that can tackle various observational limitations of the data, like finite field size, average density variations on large angular scales, plate inhomogeneities, etc. Our case, namely QSO–galaxy cross-correlation, is different from galaxy–galaxy correlation not only because two different sets of objects are being considered but also because QSOs, as opposed to galaxies, are rare; a typical field contains of the order of 10^4 galaxies down to $m_R = 20$, but only a few bright QSOs. Therefore the various refinements on the standard estimator discussed in the literature are not applicable in the present case.

The estimator that we use to compute the QSO–galaxy cross-correlation function is defined by

$$\omega(\theta) = \frac{D_{\rm Q}D_{\rm G}}{\langle R'_{\rm Q}D_{\rm G}\rangle} - 1, \qquad (1)$$

where $D_{\rm Q}D_{\rm G}$ is the actual number of QSO–galaxy pairs of a given separation, and $R'_{\rm Q}D_{\rm G}$ is the number of random QSO–real galaxy pairs. Random QSO positions are obtained for every real QSO by randomly 'scattering' it in the *azimuthal* direction with respect to the field centre, while keeping its radial distance the same. This estimator deals successfully with the problem of low QSO numbers, our circular field boundaries, and radial sensitivity gradients on Schmidt plates. Had we used random QSOs that were scattered in both radial and azimuthal directions (or, equivalently, in x and y), the presence of plate edges together with the small number of QSOs would have resulted in spurious correlations. Since azimuthally scattered random QSOs sample the same radius-dependent galaxy density on the plates as the corresponding real QSOs, radial plate gradients cancel out. To remind ourselves that our estimator is not the standard one, we use $R'_{\rm Q}$, instead of $R_{\rm Q}$, in equation (1). The angular brackets in the denominator of equation (1) mean that we take the average of 100 random realizations for every real QSO.

Note that for QSOs located close to plate centres, equation (1) can underestimate the absolute amplitude of the cross-correlation signal. Suppose that the plate centre happens to have a real excess or deficit of galaxies. All the randomly generated QSOs close to field centre will also be sampling the same real excess or deficit of galaxies, and thus the cross-correlation signal will not be detected. However, this is a small effect, because only a small percentage of the QSOs are close to the plate centre.

The cross-correlation as a function of angular scale, θ, is first calculated for every field separately. The final $\omega(\theta)$ is the average of individual field contributions, weighted by the number of QSOs they contain. We do not attempt to estimate correlations on scales larger than a single plate, i.e., $\theta \gtrsim 4°$.

To test our estimator, we calculate the cross-correlation signal between galaxies (extended objects) and Galactic stars (star-like objects), both taken from the red APM plates. In this particular example, galaxies are confined to a magnitude range between 18.5 and 20.0, while stars have magnitudes between 17.0 and 18.0. The surface density of these objects as a function of the distance from plate centre, averaged over 11 plates, is shown in the top panel of Fig. 2. The empty circles are galaxies, and filled circles are stars. Both types of objects show radial gradients. The star–galaxy cross-correlation estimated using equation (1) is represented as star symbols in the lower panel of the same figure. The cross-correlation

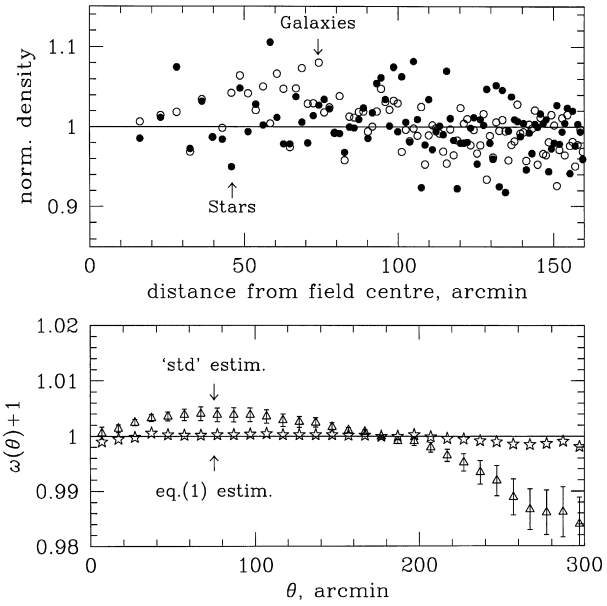

Figure 2. Top panel: normalized radial number density of $18.5 \leq m_R \leq 20.0$ APM galaxies around plate centres, summed over 11 equatorial fields (empty circles), and $17.0 \leq m_R \leq 18.0$ APM stars (filled circles). Both types of objects show radial density gradients. Bottom panel: cross-correlation between stars and galaxies using equation (1) (star symbols) and 'standard' (triangles) estimators. The 1σ error bars, estimated as the standard deviation of the mean of 11 LBQS fields, are plotted in the latter case. Note that the horizontal scale in the bottom panel is twice as long as in the top panel, since separations as large as the plate diameter can be considered.

estimated using the standard method, i.e., by scattering random QSOs in the x and y directions, is shown as triangles. The estimator defined by equation (1) has successfully compensated for galaxy and star radial gradients; its application shows that there is no correlation between stars and galaxies, as expected. On the other hand, the standard estimator's results are dominated by spurious effects. We therefore use the estimator defined by equation (1) in the rest of this paper.

3.2 Results of cross-correlation

Now we estimate QSO–galaxy correlations using one subset of QSOs, and different galaxy subsamples defined by their apparent magnitudes. As a check, for every QSO–galaxy correlation we calculate QSO–star correlation, with stars in the same magnitude range as galaxies.

Fig. 3 shows QSO–galaxy (top panel) and QSO–star (bottom panel) cross-correlation for QSOs with $z \geq 1$ and $m \leq 18$, and four galaxy subsamples, all taken from the red plates, with magnitude ranges:

16.00–19.50 (empty circles),
17.32–19.68 (triangles),
18.50–20.00 (solid circles),
19.54–20.46 (stars).

The bin widths were chosen such that the number of galaxies per bin is approximately the same in all bins. The QSO–galaxy cross-correlation signal, $\omega_{\rm QG}(\theta)$, is detected clearly, while Galactic stars do not correlate with QSOs, as expected. The signal persists to separations of ~75 arcmin; beyond that the slope of $\omega_{\rm QG}(\theta)$

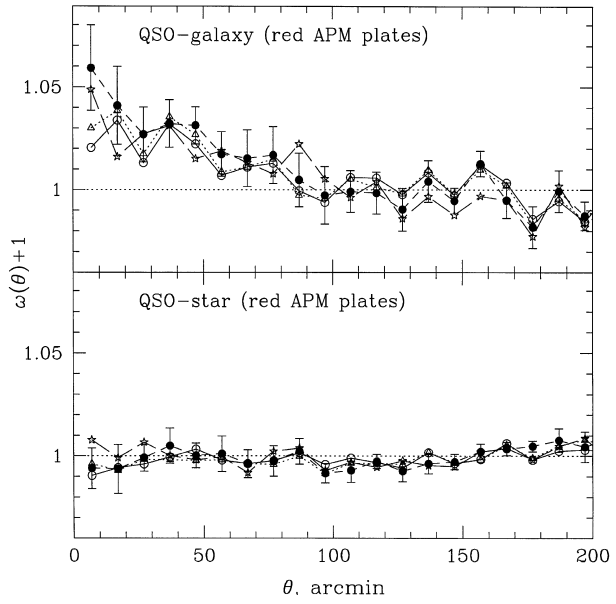

Figure 3. QSO–galaxy (top) and QSO–star (bottom) correlations using the same QSO subsample ($z \geq 1$, $m \leq 18.0$) and four galaxy subsamples taken from the *red* APM plates, with magnitude ranges: 16.00–19.50 (empty circles), 17.32–19.68 (triangles), 18.50–20.00 (solid circles) and 19.54–20.46 (stars). Error bars are 1σ standard deviation of the mean of 11 LBQS fields, and are shown only for the $18.50 \leq m_R \leq 20.00$ case.

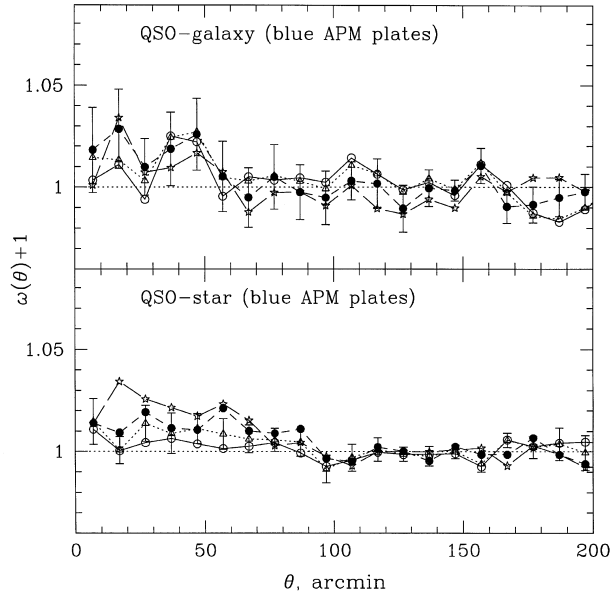

Figure 4. QSO–galaxy (top) and QSO–star (bottom) correlations using the same QSO subsample ($z \geq 1$, $m \leq 18.0$) and four galaxy subsamples taken from the *blue* APM plates, with magnitude ranges: 17.50–21.00 (empty circles), 18.82–21.18 (triangles), 20.00–21.50 (solid circles) and 21.04–21.96 (stars). Error bars are 1σ standard deviation of the mean of 11 LBQS fields, and are shown only for the $20.00 \leq m_R \leq 21.50$ case.

becomes nearly zero. At $\theta \gtrsim 150$ arcmin the signal is mostly negative because of the integral constraint imposed on the correlation function. Although all four galaxy magnitude bins show comparable signal, the strongest correlations are with $18.5 \leq m_R \leq 20.0$, i.e., the 'faintest-but-one' bin. Perhaps this is not surprising: if the signal is due to weak lensing, then fainter galaxy samples, i.e., those at higher redshifts, are expected to be better lenses for QSOs at $z \geq 1$. On the other hand, the faintest magnitude bin is probably contaminated by stars, which would tend to dilute the observed $\omega_{\rm QG}$.

Fig. 4 is the same as Fig. 3, except that the galaxies here were taken from the blue plates. The magnitude ranges are:

17.50–21.00 (empty circles),
18.82–21.18 (triangles),
20.00–21.50 (solid circles),
21.04–21.96 (stars).

The apparent association between 'stars' on blue APM plates and QSOs is due to a population of compact red galaxies, which appear extended on red plates, but are stellar on blue plates. This population has an average colour of $B - R = 2.1$, much redder than typical galaxies in the 18.5 to 20.0 magnitude range detected on the red plates. The existence of this population of galaxies is known, and preliminary spectroscopic work indicates that these are ellipticals at a typical redshift of 0.3 (Hewett et al. 1998). Recently, a faint lensed arclet of a high-redshift source has been observed centred on one of these galaxies (Hewett et al. 1998). This population of compact red ellipticals at $z \sim 0.3$ is also an important contributor to the weak lensing induced correlation between QSOs and galaxies. Because these galaxies appear stellar on blue APM plates, a positive correlation between QSOs and 'stars' is detected on these plates (Fig. 4, bottom panel). Also, because this population is not detected as 'galaxies' on blue plates, the corresponding QSO–galaxy correlation (Fig. 4, top panel) is weaker compared to that on the red plates. Because of these factors affecting the blue APM plates,we will use only red plates in the rest of the analysis.

Before we proceed, it is important to note that the amplitude of the signal that we measure here is a lower limit to the true signal because of three effects. First, as explained above (Section 3.1), our cross-correlation estimator can bias the amplitude of the signal low. Second, because QSO candidates for the LBQS were selected using prism plates, candidates in crowded areas, e.g., high galaxy density, are more likely to be rejected as their spectra have a higher chance of being 'corrupted' by a superimposed galaxy image. Third, APM object classifier and estimated object magnitudes are not perfect, and hence any true signal which is due to galaxies in any given magnitude range will be diluted by stars and by objects of other apparent magnitudes.

3.3 Integrated correlations for $\theta < 75$ arcmin

In the previous section we used one subsample of QSOs. To eliminate any bias related to that particular choice of QSO properties, we extend the QSO–galaxy cross-correlation analysis to a range of QSO subsamples, each having a minimum redshift and limiting apparent magnitude, $z_{\rm Q,\,min}$ and $m_{\rm Q,\,lim}$. For each subsample we calculate the integrated correlation amplitude within $\theta = 75$ arcmin, i.e., we characterize each ($z_{\rm Q,\,min}$, $m_{\rm Q,\,lim}$) subsample by one number. This integrated correlation amplitude is plotted as a contour plot in Fig. 5.

The top two panels of Fig. 5 show the contours of constant QSO–galaxy correlation amplitude (left-hand panel) and statistical significance (right-hand panel), while the bottom two panels are the same, but for QSO–star correlations. The correlation contours are drawn at 0.98 and 0.99 (thick and thin dashed lines), and 1.02 and 1.01 (thick and thin solid lines) levels. The significance contours are at 90 and 99 per cent (thick and thin lines). The significance level is the fraction of synthetic QSO subsamples, out a total of 100, that show correlations weaker that the corresponding real QSO

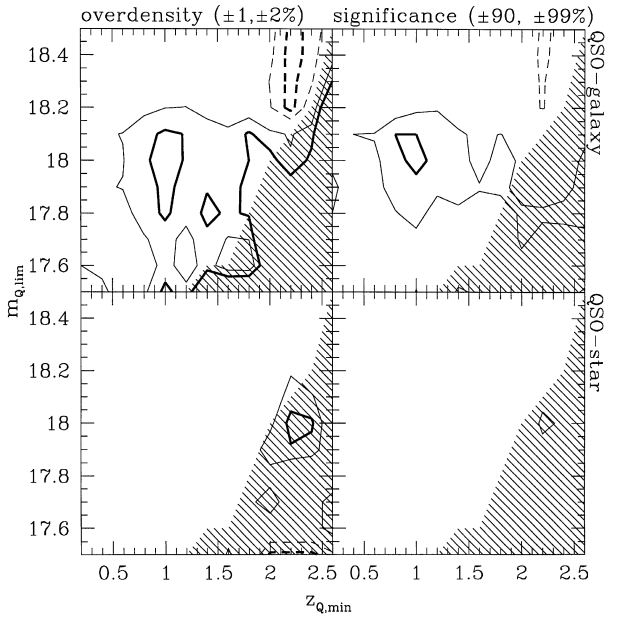

Figure 5. Contour plots of cumulative ω_{QG} and ω_{QS} for $\theta \leq 75$ arcmin (left), and the corresponding statistical significance (right). The correlation contours are drawn at 0.98 and 0.99 (thick and thin dashed lines), and 1.02 and 1.01 (thick and thin solid lines) levels. The significance contours are at 90 and 99 per cent (thin and thick lines). Note that APM stars show no correlation with QSOs.

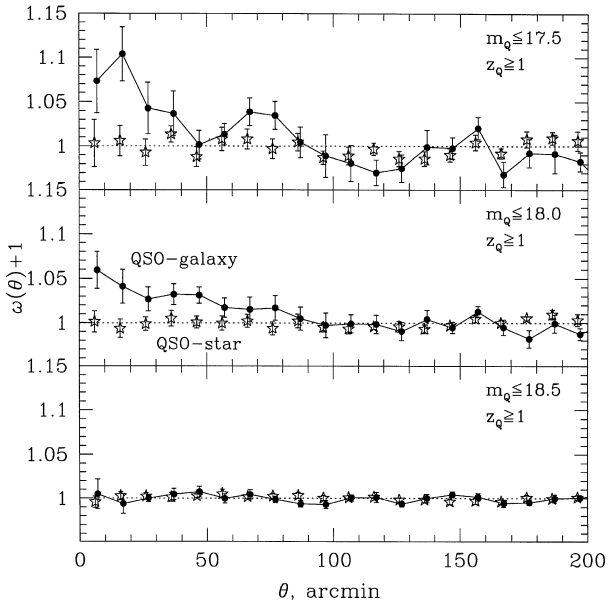

Figure 6. QSO–galaxy (solid dots and lines) and QSO–star (star symbols) cross-correlation function. The galaxies are taken from the red APM plates, and have magnitudes between 18.5 and 20.0. Results for three QSO subsamples are presented, as indicated in the upper right corner of each panel. Note that the amplitude of ω_{QG} increases rapidly for brighter QSOs.

subsample. This estimate makes no a priori assumptions about the distribution of errors. The right-hand corner of each panel is shaded where the number of QSOs per subsample is less than 10; so, even if the correlations appear significant, they should be regarded with caution, because not enough QSOs are being averaged over.

It is apparent from Fig. 5 that QSO–galaxy correlations are statistically significant for some QSO subsamples, whereas no significant correlations, above 90 per cent confidence level, are detected between QSOs and Galactic stars. Because of the null result for QSO–star and star–galaxy (Fig. 2) correlations, we conclude that QSO–galaxy signal is real, and not an artefact of plate sensitivity gradients, etc.

What are the possible causes of these correlations? The correlations cannot be due to physical QSO–galaxy associations, because of the QSO/galaxy redshift mismatch. Another possibility is that patchy Galactic obscuration 'creates' galaxy and QSO overdensities, which are then necessarily correlated. This hypothesis can be ruled out, because the observed correlations show a strong variation with $z_{Q,\,min}$ both in amplitude and significance, whereas dust would not be able to differentiate between QSOs at different redshifts. Furthermore, the fluctuations in the distribution of Galactic dust are not extreme enough to produce the observed variations in galaxy and QSO number densities. The rms fluctuations in obscuration in these high galactic latitude ($|b| \gtrsim 45°$) LBQS fields is typically 0.1 mag in B (Burstein & Heiles 1978; Schlegel et al. 1998), which would produce rms fluctuations in projected galaxy density of a factor of 1.07, while the observed rms value is 4 on ~10-arcmin scales, and 1.4 on 1° scales. Thus the observed galaxy density fluctuations in these APM fields are primarily due to galaxy clustering, and not to patchy Galactic dust obscuration. Therefore we conclude that the correlations are not due to dust.

The only remaining explanation is the weak gravitational lensing of the background QSOs by the matter associated with the APM galaxies. This interpretation is supported by the trends seen in the top panels of Fig. 5. The correlations are strongest with QSOs at $z \gtrsim 1$, consistent with theoretical expectations (Dolag & Bartelmann 1997; Sanz et al. 1997). The apparent magnitude-dependent behaviour of the correlations is also consistent with the lensing interpretation; ω_{QG} is strongest for $m_Q \leq 18$. At fainter magnitudes the slope of the QSO luminosity function becomes shallower, and so amplification bias, and hence correlation strength, become less pronounced. At magnitudes much brigher than ~18 the significance of the QSO–galaxy correlations is low due to small QSO numbers.

As an example of the actual ω_{QG} as a function of separation, Fig. 6 shows the correlation between $z \geqslant 1$ QSOs and galaxies, for three different $m_{Q,\,lim}$; 17.5, 18.0 and 18.5. The star symbols are QSO–star correlations, and the solid dots are QSO–galaxy correlations. The error bars are 1σ standard deviation of the mean of 11 LBQS fields. The results shown in the middle panel, $m_Q < 18$, are the same as solid circles in Fig. 3.

4 ANALYSIS AND COMPARISON WITH PREDICTIONS

Having measured the weak lensing induced two-point correlation function between QSOs and galaxies, we now compare it to theoretical expectations, using two approaches (Sections 4.1 and 4.2) that differ mostly in the method used to testimate the clumpiness of the mass responsible for lensing. The results of these two approaches are compared to each other and to the observations. As observations, we chose the correlations presented in the middle panel of Fig. 6, i.e., for a QSO subsample with $z_Q \geq 1$ and $m_Q \leq 18.0$. We plot these as filled circles in Fig. 7, for separations where the amplitude of ω_{QG} remains consistently positive.

4.1 Phenomenological predictions

The main assumption here is that the mass distribution responsible

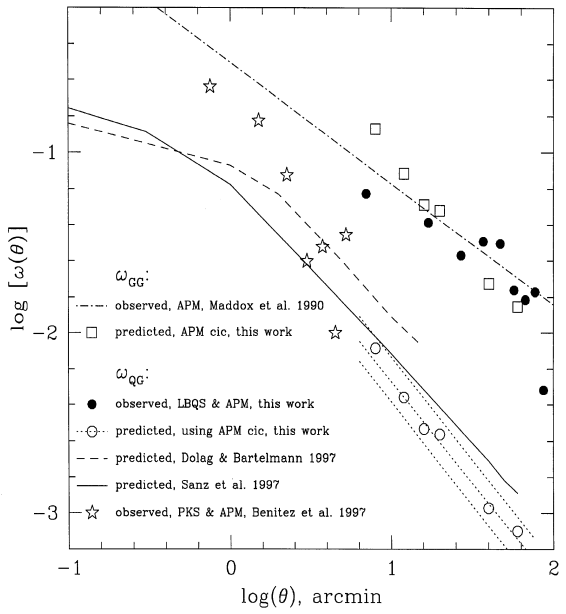

Figure 7. Observed and predicted QSO–galaxy correlations; note the log–log scale. The different lines and points are described in the figure. The solid dots represent the $z \geq 1$ and $m \leq 18.0$ QSO subsample. See Sections 4.1 and 4.2 for details.

for lensing is traced by the observed galaxies in the nearby Universe. The total 'thickness' of the lensing material can be estimated from the galaxy redshift distribution and an assumed Ω_0, while the distribution of fluctuations on any given scale is obtained from the counts-in-cells distribution of the APM galaxies.

First, we estimate the amount of matter associated with the observed APM galaxies, i.e., we calculate the optical depth for sources located at the redshift of the QSOs,

$$\tau_{\rm APM} = \rho_{\rm crit}\,\Omega_0 \int_0^{z_{\rm max}} \frac{(c{\rm d}t/{\rm d}z)(1+z)^3}{\Sigma_{\rm crit}(z, z_{\rm s})}\,{\rm d}z, \qquad (2)$$

Here, $c{\rm d}t$ is the thickness of the lensing slice at redshift z, $\rho_{\rm crit}\,\Omega_0(1+z)^3$ is its mass density, and $\Sigma_{\rm crit}(z, z_{\rm s})$ is the critical lensing surface mass density at z for a source at $z_{\rm s}$. The latter is assumed to be 1.5, the average redshift of our QSO subsample. We assume an open universe with $\Omega_0 = 0.3$. The upper limit of integration, $z_{\rm max}$, is taken to be the redshift at which the APM galaxy redshift distribution (Fig. 1) drops to half of its peak value; $z_{\rm max}$ is about 0.33. In other words, we assume that the optical depth of the mass traced by the APM galaxies is the total optical depth up to a redshift of 0.33. Since the particular choice of $z_{\rm max}$ is somewhat arbitrary, we also quote results for $z_{\rm max} = 0.28$ and 0.39, corresponding to redshifts where the APM galaxy redshift distribution drops to 3/4 and 1/4 of its peak value respectively. The corresponding range of $\tau_{\rm APM}$ values is from 0.012 to 0.021, while for $z_{\rm max} = 0.33$ it is 0.016.

Next, we assume that on scales larger than a few arcminutes the APM galaxies trace the total matter distribution (up to $z_{\rm max}$) with a biasing factor b. The projected galaxy clustering is described by the scale-dependent counts-in-cells distribution of the APM galaxies, $p(\sigma|\theta){\rm d}\sigma$, where σ is the galaxy number density normalized by the average density. A patch of sky with density σ produces an amplification $A(\sigma) \approx 1 + 2\tau_{\rm APM}(\sigma - 1)/b$, in the weak lensing limit. The corresponding over-density of QSOs background to this patch is given by

$$q(\sigma) = A^{2.5\alpha-1} \approx 1 + (2\tau_{\rm APM}[\sigma - 1]/b)(2.5\alpha - 1), \qquad (3)$$

where α is the slope of the QSO number counts; $\langle\alpha\rangle = 1.1$ for our QSO subsample.

The cross-correlation between QSOs and galaxies is then estimated as

$$\omega_{\rm QG}(<\theta) + 1 \approx \int_0^\infty p(\sigma|\theta) q(\sigma)\sigma\,{\rm d}\sigma. \qquad (4)$$

The galaxy autocorrelation function is given by an equation similar to equation (4):

$$\omega_{\rm GG}(<\theta) + 1 \approx \int_0^\infty p(\sigma|\theta)\sigma^2\,{\rm d}\sigma. \qquad (5)$$

The ratio of $\omega_{\rm QG}$ to $\omega_{\rm GG}$ can be derived analytically, in the weak lensing regime. Making use of the fact that $p(\sigma|\theta)$ is a normalized probability distribution with an average of σ equal to 1, the ratio of equation (4) to equation (5) gives

$$\omega_{\rm QG}(\theta) \approx (2\tau_{\rm APM}/b)(2.5\alpha - 1)\omega_{\rm GG}(\theta), \qquad (6)$$

This equation applies if the same galaxy counts-in-cells distribution is used to calculate $\omega_{\rm QG}(\theta)$ and $\omega_{\rm GG}(\theta)$, and gives the QSO–galaxy correlation amplitude due to lensing by these galaxies only.

For $\tau_{\rm APM} = 0.016$ (i.e., $z_{\rm max} = 0.33$), $b = 1$, $\langle\alpha\rangle = 1.1$, the ratio $\omega_{\rm QG}/\omega_{\rm GG} \approx 0.056$. Galaxy autocorrelation function from the APM galaxies was calculated by Maddox et al. (1990), and is plotted as dot-dashed line in Fig. 7. The amplitude of $\omega_{\rm GG}$ is appropriate for the galaxy magnitude range used here. With this $\omega_{\rm GG}$, QSO–galaxy cross-correlation function should lie 1.25 (in the log) below $\omega_{\rm GG}$. Since the observed $\omega_{\rm QG}$ is roughly of the same amplitude as the galaxy–galaxy correlations, the predictions based on equation (6) are a factor of 15 below observations.

As a check, equations (4) and (5) can be also applied directly to the counts-in-cells data to calculate the correlation functions at a range of separations, assuming the optical depth of the APM galaxies. The results are shown in Fig. 7, as empty squares ($\omega_{\rm GG}$) and empty circles ($\omega_{\rm QG}$). The vertical offset of the two is about a factor of 15, in agreement with equation (6). Because vertical normalization of $\omega_{\rm GG}$ scales with the magnitude of the galaxies, and the data we use were not properly magnitude-calibrated, we have adjusted the vertical normalization of these two estimated functions such that our derived $\omega_{\rm GG}$ matches that of Maddox et al. (1990).

The empty circles assume $z_{\rm max} = 0.33$; the dotted line through them is a rough fit. The upper and lower dotted lines are for $z_{\rm max} = 0.39$ and 0.28 respectively, and bracket the range of our predicted values. The model predictions cover an angular scale range of 4 arcmin to 1°; on scales smaller than 4 arcmin the number of galaxies per cell is small, and so the resultant counts-in-cells distribution is dominated by Poisson noise. Scales much larger than 1° are comparable in size to the Schmidt plates, so the derived counts-in-cells will be substantially narrower than the true distribution, because we normalize the galaxy number density to the plate's average, on each plate separately, thus ignoring any power on larger scales. For the same reason, the slope of our $\omega_{\rm GG}(\theta)$ is somewhat steeper than the commonly derived value of $\gamma \approx 0.7$ (Maddox et al. 1990).

As mentioned above, our phenomenological model predictions fall short of the observations by about a factor of 10–20. Is our model too simplistic?

4.2 Theoretical predictions from the literature

Dolag & Bartelmann (1998) and Sanz et al. (1997) used an alternative way to derive mass fluctuations in the Universe. Starting with a particular type of cosmology and an initial matter power spectrum, they used the results of a semi-analytic prescription for the non-linear evolution of the power spectrum (Peacock & Dodds 1996) to derive the spectrum of mass distribution as a function of redshift and scale. Assuming weak-lensing regime, a slope of QSO counts α, and a biasing parameter, the mass distribution spectrum was used to predict the observed QSO–galaxy correlations. These calculations were primarily motivated by an observed correlation between PKS radio-selected QSOs and APM galaxies, as derived by Benítez & Martínez-González (1997), and shown as star symbols in Fig. 7. Within their range of applicability, i.e., $\theta > 1$–2 arcmin, both analytical models reproduce the PKS-APM results well. Correlations on scales larger than 15 arcmin could not have been detected by Benítez & Martínez-González because they restricted their analysis to patches of 15-arcmin radius around each QSO.

To compare these two model predictions to our observed $\omega_{\rm QG}(\theta)$, we rescaled their results to $\alpha = 1.1$. Dolag & Bartelmann results were additionally rescaled from $h = 0.7$ to $h = 0.5$ using their fig. 4. The predictions are plotted as dashed and solid lines in Fig. 7; both are for $\Omega = 0.3$, $\Lambda = 0$. Similar to the results of the phenomenological model, the analytical models underestimate the amplitude of observed $\omega_{\rm QG}$ by a factor of 10 on large angular scales.

Since phenomenological and analytical models used different routes to arrive at $\omega_{\rm QG}$, it is encouraging that they agree reasonably well with each other. A factor of 1.5–2 discrepancy (solid and dashed lines versus dotted lines) arises probably because our phenomenological model ignored lensing by structures at $z \gtrsim 0.35$, which are not sampled by galaxies in the APM Catalogue, but are still efficient lenses for the QSOs. Turning the argument around, the small discrepancy means that nearby galaxies, $z \lesssim 0.35$, dominate the weak lensing of $z \geq 1$ QSOs.

5 DISCUSSION

In the last section we have seen that the amplitude of observed QSO–galaxy correlation is underpredicted by theoretical models. The discrepancy is a factor of 3–4 at $\theta \lesssim 10$ arcmin, and increases to a factor of 10 on degree scales.

Can a reasonable change of parameters account for such a large discrepancy? Assuming that the effects of weak lensing are dealt with correctly, and that the signal is real and is due to lensing, we are left with two possibilities (see equation 6): either the slope of the QSO number counts at $z \geq 1$ is very steep, or mass fluctuations on relevant scales, i.e., between a few and 15 Mpc, are more extreme than fluctuations in galaxy number density. The amplitude of $\omega_{\rm QG}$ is quite sensitive to the slope of the QSO number counts; however, to reproduce the observations, α would have to be $\sim$8, while the observed slope values for LBQS QSO in this redshift range lie between 0.8 and 1.5, comparable to the QSO luminosity function slopes, $\sim$1.6, derived from the LBQS (Hewett, Foltz & Chaffee 1993) in this redshift range.

Alternatively, we could require that the galaxies are antibiased with respect to the mass by a factor of $\sim$10 ($b \sim 0.1$), implying a σ_8 value of around 10, which is hard to reconcile with any gravitational clustering scenario, and observations of the large-scale structure. The value of $\Omega^{0.6}\sigma_8$ is well constrained by the abundance of galaxy clusters; White, Efstathiou & Frenk (1993) estimate $\Omega^{0.6}\sigma_8$ to be $\sim$0.6. Based on cluster peculiar velocities, Watkins (1997) derives $\Omega^{0.6}\sigma_8$ to be 0.44. Thus an $\sigma_8 \sim 10$ would require an Ω so low, it would just agree with $\Omega_{\rm baryon}$ from primordial nucleosynthesis constraints (Hogan 1996), but would strongly contradict dynamical measurements on cluster scales ($\Omega = 0.24$; Carlberg et al. 1996), and power spectrum shape parameter constraints ($\Gamma = \Omega h = 0.2$–0.3; Maddox et al. 1996). Furthermore, such a high σ_8 value is ruled out by the recent direct estimation by Fan, Bahcall & Cen (1998), who compute $\sigma_8 = 0.83 \pm 0.15$ from the redshift evolution of galaxy clusters.

A combination of factors, for example, $b = 0.3$ and $\alpha = 2.3$ shares the burden between the two observables, but is still quite unpalatable. In fact, it is difficult to see how any reasonable change of parameters or assumptions can bring these up to the observed amplitude of $\omega_{\rm QG}$ on $\sim$degree scales.

If the explanation does not lie with either the lensers or the lensees, then maybe the lensing process has to be looked at more carefully. It is conceivable, for example, that some hitherto unexplored non-linearities in the description of light propagation through a clumpy universe could be responsible.

At present, the factor of 10 discrepancy between observations and predictions remains unaccounted for.

6 IMPLICATIONS FOR OBSERVATIONAL COSMOLOGY

The results of the correlations described above have interesting implications for the observed distribution and properties of certain types of high-redshift sources. Here we explore a few of these.

The results imply that the projected density of foreground structure affects the density of high redshift objects. To quantify this statement in the case of QSOs, our results can be represented as a plot of QSO number density as a function of foreground galaxy density on a given angular scale. To do that, we randomly lay down a large number of circular patches over LBQS fields. In each patch we calculate galaxy number density. For all patches of a given galaxy density we then calculate the average QSO density, and repeat the process for several values of galaxy density. The results are shown in Fig. 8, using patches of radius 12 arcmin, and three QSO subsamples, all with $z_{\rm Q} \geq 1$. The error bars are 1σ standard deviations of the mean of 10 different realizations of the experiment just described.

It is seen that the observed projected density of QSOs is a function of the foreground galaxy density, in the sense that bright QSOs are found preferentially in the directions of over-dense galaxy regions; for example, a $m_{\rm Q} \leq 17.5$, $z_{\rm Q} \geq 1$ optically selected QSO is twice as likely to be found in the direction where the galaxy density is 1.5 times the average. However, QSOs are not the only class of objects affected by weak lensing on large scales. Any population of high-redshift objects, whose number counts slope is substantially different from 0.4 will be affected in a similar fashion. Intrinsically bright galaxies, those on the exponential part of the Schechter luminosity function (Schechter 1976), confined to a narrow redshift range, are an example. As indicated in Fig. 8, both under- and over-densities of background sources can be expected. Thus this bears direct relevance to the *Hubble Deep Field* (Williams et al. 1996), which was intentionally chosen to lie in the direction of the sky devoid of nearby, $z \lesssim 0.3$, structure (the nearest galaxy cluster is 48 arcmin away, etc.). Depending on the exact underdensity of nearby galaxies in the HDF, and the intrinsic luminosity of high-redshift galaxies, the latter can be depleted by a factor of up to 5.

A further implication is that the rms dispersion in the observed luminosities of standard candles, and observed sizes of standard

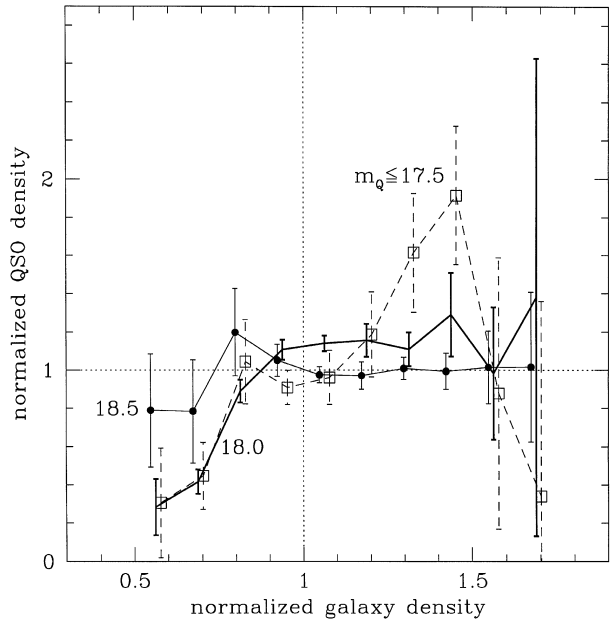

Figure 8. Normalized QSO density for a given normalized galaxy density, in circular patches of radius 12 arcmin. See Section 6 for details. Galaxies are $18.5 \leq m_R \leq 20.0$; QSOs are at $z \geq 1$. Bright QSOs are more likely to be found in the directions over-dense in nearby galaxies, and avoid directions of lower than average galaxy densities.

rulers at high redshift would be somewhat larger than currently predicted from numerical simulations of the lensing effects (Wambsganss et al. 1997). A rough extrapolation from our results shows that the rms dispersion in amplifications would be 0.1–0.2 mag, comparable to the light-curve shape corrected dispersion in the luminosities of four $z \sim 1$ supernovae of Type Ia (Garnavich et al. 1998), but smaller than the dispersion in sizes of compact radio sources (Kellerman 1993) and double-lobed radio sources (Buchalter et al. 1998). The fact that the rms dispersion in these observed quantities is comparable to or larger than what is implied by our weak lensing analysis means that the rms spread in lensing-induced amplifications is not usefully constrained by the current samples of standard candles and rulers. Because the weak lensing induced dispersion in the observed quantities is not Gaussian (or even symmetric), the overall trend with redshift can also be affected (see also Wambsganss et al. 1997).

Another aspect of extragalactic astronomy that is affected by weak lensing is the density and redshift evolution of Lyα forest clouds. It is evident from Fig. 8 that bright, high-redshift QSOs do not sample random lines of sight, as is generally hoped in the studies of intervening QSO Lyα absorption lines. Since the most efficient lenses for a wide range of source redshifts are at $z_l \lesssim 0.6$, one would expect a corresponding increase in the detected density of high equivalent width Lyα forest clouds, which are known to be loosely associated with galaxies (Lanzetta et al. 1995; Stocke et al. 1995; Bowen, Blades & Pettini 1996) at these redshifts. An increase in dN/dz at $z \lesssim 1$ compared to a power-law extrapolation from higher redshifts has been detected (Bahcall et al. 1993; Impey et al. 1996); a substantial contribution to this increase is probably due to weak lensing of back-lighting QSOs.

7 CONCLUSIONS

We have found that bright, high-redshift, optically selected LBQS QSOs are positively correlated with foreground APM galaxies. The cross-correlations are significant and are neither physical in nature nor a result of patchy Galactic obscuration. The most plausible explanation, which is also supported by the qualitative behaviour of the correlations, is weak gravitational lensing of the background QSOs by the intervening dark matter traced by the APM galaxies. However, the amplitude of correlations on degree scales, or ~10–15 Mpc at the redshift of the lenses, is a factor of 10 higher than predicted from models. The discrepancy is hard to reconcile with what we currently believe to be true about the Universe.

The implications of the effects of weak lensing for the observed high-redshift Universe are far-reaching, and so it is imperative to study such correlations further using other large, uniform data sets. An analysis with radio-selected high-redshift sources would be ideal, as these sources are immune to the effects of Galactic dust obscuration. Samples of high-redshift sources, both optical and radio, observed down to faint flux limits would be useful, as both positive correlations and anticorrelations with foreground galaxies are expected, depending on the limiting flux of the source sub-sample.

Finally, it is interesting to note that the QSO–galaxy correlations described here are probing the physical scale where the galaxy power spectrum is observed to have a kink, corresponding to a primordial feature in the true linear power spectrum, which is not reproduced by any variants of the CDM model (Peacock 1997).

ACKNOWLEDGMENTS

LLRW thanks Steve Maddox for useful discussions on the APM Catalogue and correlation functions, and also acknowledges the support of PPARC fellowship at the Institute of Astronomy, Cambridge.

REFERENCES

Bahcall J. N. et al., 1993, ApJS, 87, 1
Bartelmann M., Schneider P., 1993, A&A, 271, 421
Bartelmann M., Schneider P., 1994, A&A, 284, 1
Bartelmann M., Schneider P., Hasinger G., 1994, A&A, 290, 399
Benítez N., Martínez-Gonzáles E., 1995, ApJ, 448, L89
Benítez N., Martínez-Gonzáles E., 1997, ApJ, 477, 27
Bowen D. V., Blades J. C., Pettini M., 1996, ApJ, 464, 141
Boyle B. J., Fong R., Shanks T., 1988, MNRAS, 231, 897
Broadhurst T. J., 1994, in Holt S. S., Bennett C. L., eds, Proc. of the 5th Annual Astrophysics Conf., College Park, Maryland, p. 320
Broadhurst T. J., Taylor A. N., Peacock, J. A., 1995, ApJ, 438, 49
Buchalter A., Helfand D. J., Becker R. H., White R. I., 1998, ApJ, 494, 503
Burstein D., Heiles C., 1978, ApJ, 225, 40
Carlberg R. G., Yee H. K. C., Ellingson E., Abraham R., Gravel P., Morris S., Pritchet C. J., 1996, ApJ, 462, 32
Dolag K., Bartelmann M., 1997, MNRAS, 291, 446
Fan X., Bahcall N. A., Cen R., 1998, preprint
Ferraras I., Benítez N., Martínez-González E., 1997, AJ, 114, 1728
Fugmann W., 1990, A&A, 240, 11
Garnavich P. M. et al., 1998, ApJ, 493, L53
Hamilton A. J. S., 1993, ApJ, 417, 19
Hewett P. C., 1982, MNRAS, 201, 867
Hewett P. C., Harding M. E., Webster R. L., 1991, in Kayser R., Schramm T., Nisser L., eds, Gravitational Lenses. Springer-Verlag, p. 209
Hewett P. C., Foltz C. B., Chaffee F. H., 1993, ApJ, 406, L43
Hewett P. C., Foltz C. B., Chaffee F. H., 1995, AJ, 109, 1498
Hewett P. C. et al., 1998, MNRAS, submitted
Hogan C. J., 1996, Contribution to the Princeton meeting, 'Critical Dialogues in Cosmology', astro-ph/9609138

Impey C. D., Petry C. E., Malkan M. A., Webb M. J., 1996, ApJ, 463, 473
Irwin M., Maddox S. J., McMahon R. G., 1994, Spectrum, 2, 14
Kellerman K. I., 1993, Nat, 361, 134
Lanzetta K., Bowen D. V., Tytler D., Webb J. K., 1995, ApJ, 442, 538
Maddox S. J., Efstathiou G., Sutherland W. J., Loveday J., 1990, MNRAS, 242, 43
Maddox S. J., Efstathiou G., Sutherland W. J., 1996, MNRAS, 283, 1227
Metcalfe N., Shanks T., Fong R., Roche N., 1995, MNRAS, 273, 257
Narayan R., 1989, ApJ, 339, L53
Narayan R., 1991, in Kayser R., Schramm T., Nieser L., eds, Gravitational Lenses. Springer-Verlag, p. 264
Peacock J. A., 1997, MNRAS, 284, 885
Peacock J. A., Dodds S. J., 1996, MNRAS, 280, L19
Peebles P. J. E., 1980, The Large Scale Structure of the Universe. Princeton Univ. Press, Princeton
Rodrigues-Williams L. L., Hogan C. J., 1994, AJ, 107, 451
Sanz J. L., Martínez-Gonzáles E., Benítez N., 1997, MNRAS, 291, 418
Schechter P. L., 1976, ApJ, 203, 297
Schlegel D. J., Finkbeiner D. P., Davis M., 1998, preprint
Seitz S., Schneider P., 1995, A&A, 302, 9
Stocke J. T., Shull J. M., Penton S., Donahue M., Carilli C., 1995, ApJ, 451, 24
Wambsganss J., Cen R., Xu G., Ostriker J. P., 1997, ApJ, 475, L81
Watkins R., 1997, MNRAS, 292, L59
White S. D. M., Efstathiou G., Frenk C. S., 1993, MNRAS, 262, 1023
Williams R. E. et al., 1996, AJ, 112, 1335
Wu X.-P., Han J., 1995, MNRAS, 272, 705